CROSS–POLAR MAGNETOSPHERIC PLASMA DRIFT AS OBSERVED BY CLUSTER EDI: STATISTICAL RESULTS

M. Förster[1], S. Haaland[2], G. Paschmann[3], J. B. Baker[4], H. Vaith[5], J.M. Quinn[5], and R. B. Torbert[5]

[1]*Max-Planck Institute for Extraterrestrial Physics, Garching, Germany*
[2]*Department of Physics, University of Bergen, Bergen, Norway*
[3]*International Space Science Institute, Bern, Switzerland*
[4]*Applied Physics Laboratory, Johns Hopkins University, Laurel, Maryland, USA*
[5]*University of New Hampshire, Durham, NH, USA*

ABSTRACT

The Electron Drift Instrument (EDI) measures the drift velocity of artificially injected electron beams transverse to the magnetic field. EDI operates well in low-density plasma regions, provided the magnetic field above 20 nT and the wave activity level and natural keV electron fluxes are not too high. Therefore, EDI is well suited for plasma drift measurements above the polar cap regions. The paper presents statistical patterns of polar cap convection for various solar wind conditions as obtained during the years 2001-2004.

Key words: Magnetospheric convection, Polar cap, Statistics.

1. INTRODUCTION

The convecting magnetospheric plasma at high geomagnetic latitudes is subject to a highly variable and nearly continuous energy and momentum transfer from the solar wind. The main driving process is reconnection both at the frontside magnetopause and in the geomagnetic tail, but also viscous transport at the low-latitude boundary layer (LLBL) just inside the magnetopause plays a role. The effects of reconnection are certainly more showy than those of viscosity [1]. Size and direction of the convection electric field, as well as the closely related field-aligned current (FAC) system, its extension and intensity, are all intimately correlated with the solar wind conditions, in particular with the direction of the interplanetary magnetic field (IMF).

On the other hand, the ionospheric footpoint of the magnetic field line impose the other stringent boundary condition for global current flow and convection. Any activity and magnetic field stresses imposed are communicated with the Alfvén speed between the various magnetospheric regions and the ionosphere and vice versa. Magnetospherically imposed electric potential and in particular its fluctuations are an important heat source (Joule heating) for the high-latitude thermosphere.

The high-altitude polar cap area with often very low plasma densities and relatively high magnetic field strength is well suited for EDI measurements. So we use electric field measurements obtained with EDI onboard the Cluster satellites. A previous study on EDI observations revealed the occurence of large-amplitude oscillations above the polar cap area that are superimposed on the background large-scale convection. Further it was shown that one type of fluctuations appears to grow when approaching the dayside magnetopause [2].

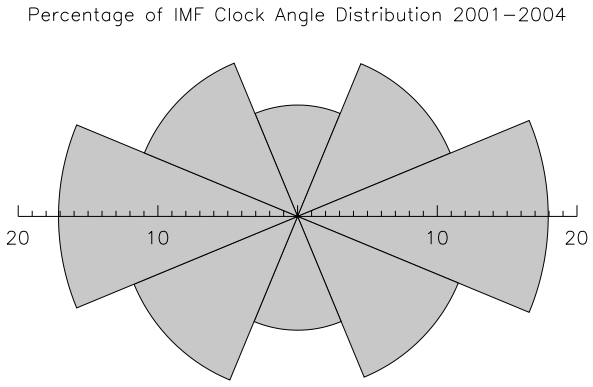

Figure 1. Relative ratio of data point numbers in each sector of the IMF clock dial diagram (in per cent) for the statistical analysis 2001–2004 of this study.

[3] used EDI data to study the average tail lobe convection further tailward of the Earth's magnetosphere. The data confirm the convection pattern toward the neutral sheet in the meridional (XZ) plane. The convection direction in the plane perpendicular to the Sun-Earth line (YZ plane) is controlled by the B_y^{IMF} component and

Proceedings Cluster and Double Star Symposium – 5th Anniversary of Cluster in Space, Noordwijk, The Netherlands, 19 - 23 September 2005 (ESA SP-598, January 2006)

the B_z^{IMF} determines the magnitude of the average convection velocity. According to their findings, convection becomes strongest for southward IMF and a dawnward component appears.

2. SOLAR WIND CONDITIONS

Solar wind conditions are the most important driver for magnetospheric convection because the interplanetary magnetic field (IMF) interacts directly with the dayside magnetic field through magnetic reconnection. But also internal processes like substorms (nightside reconnection) give substantial contributions to the magnetospheric convection pattern.

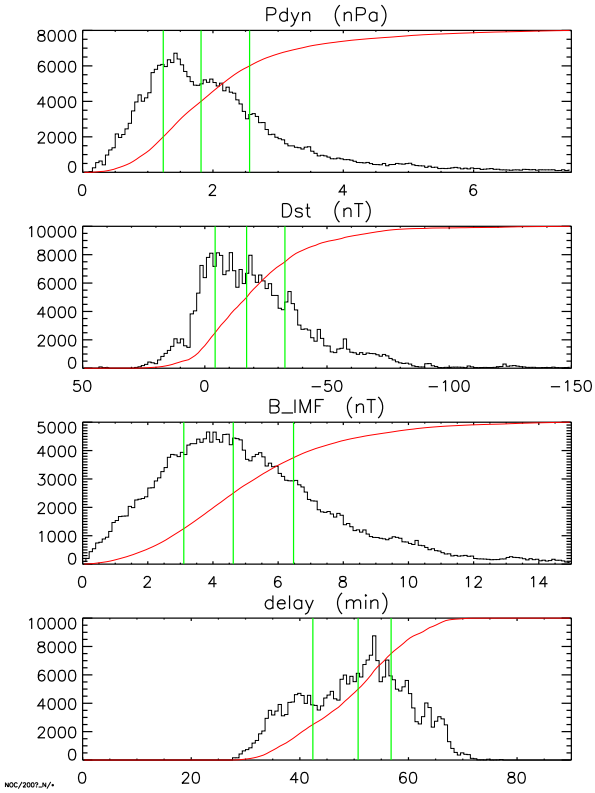

Figure 2. Distribution functions for some parameters used for the statistical analysis 2001–2004 of this study. The vertical lines indicate the quartiles of the distribution and the red lines are the accumulated values.

The correct estimation of the propagation delay time for the solar wind parameters (IMF and bulk flow) as measured by the ACE satellite near the L1 point to the magnetosphere of the Earth is an important key element of this study. The solar wind parameter are not only used for binning the data according to various conditions, but they are also used as input parameters for the magnetic field model by virtue of which the mapping of the EDI drift vector observations onto a common reference level is performed. For this provisional first study the simple convection (or advection) technique has been used, i.e., Δt is found by dividing the separation distance in $x_{GSE}-$direction by the radial solar wind velocity. This will be improved in forthcoming data analysis by use of the [4] method of solar wind phase front determination.

The primary sorting of the drift measurements is performed with respect to the IMF clock angle, defined as $\arctan(B_y^{IMF}/B_z^{IMF})$. We use eight different clock angle ranges (sectors) which are each $45°$ wide, starting with sector 0 for positve B_z^{IMF} and proceeding clockwise in the (YZ) GSM plane. The clock angle distribution of the IMF vector show clear maxima for the sectors number 2 and 6 (see Fig. 1), i.e., the magnetic field is preferentially in the ecliptical plane. The distribution functions for some of the main solar wind and geomagnetic parameters are shown in Fig. 2.

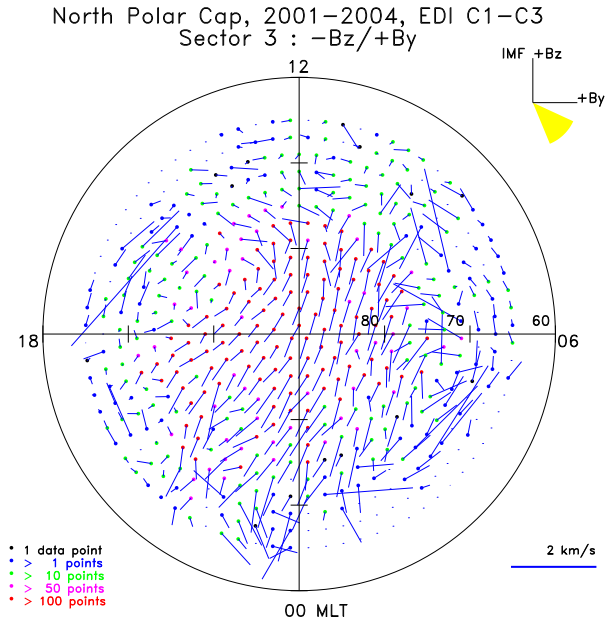

Figure 3. North polar cap drift vector plot of mapped EDI in-situ drift measurements (2001–2004) for sector 3 of the IMF clock dial diagram, i.e., clock angle around $135° \pm 22.5°$ ($+B_y^{IMF}$ and $-B_z^{IMF}$).

3. DATA PROCESSING

The four satellites of the Cluster mission were launchend in summer 2000 into a highly elliptical polar orbit. Perigee and apogee of the bundled Cluster orbits are close to the ecliptical plane at about 4 R_E and 19 R_E, respectively. The satellites traverse the area above the polar caps along their slant orbital pieces between the auroral zone and the more distant magnetospheric regions or the magnetopause (or vice versa) at various altitutes. A large fraction of this area is occupied by open magnetic field lines that form further tailward the magnetospheric lobes. Due to orbital precession, all local times above the polar cap areas are covered twice per year with overflights at different heights.

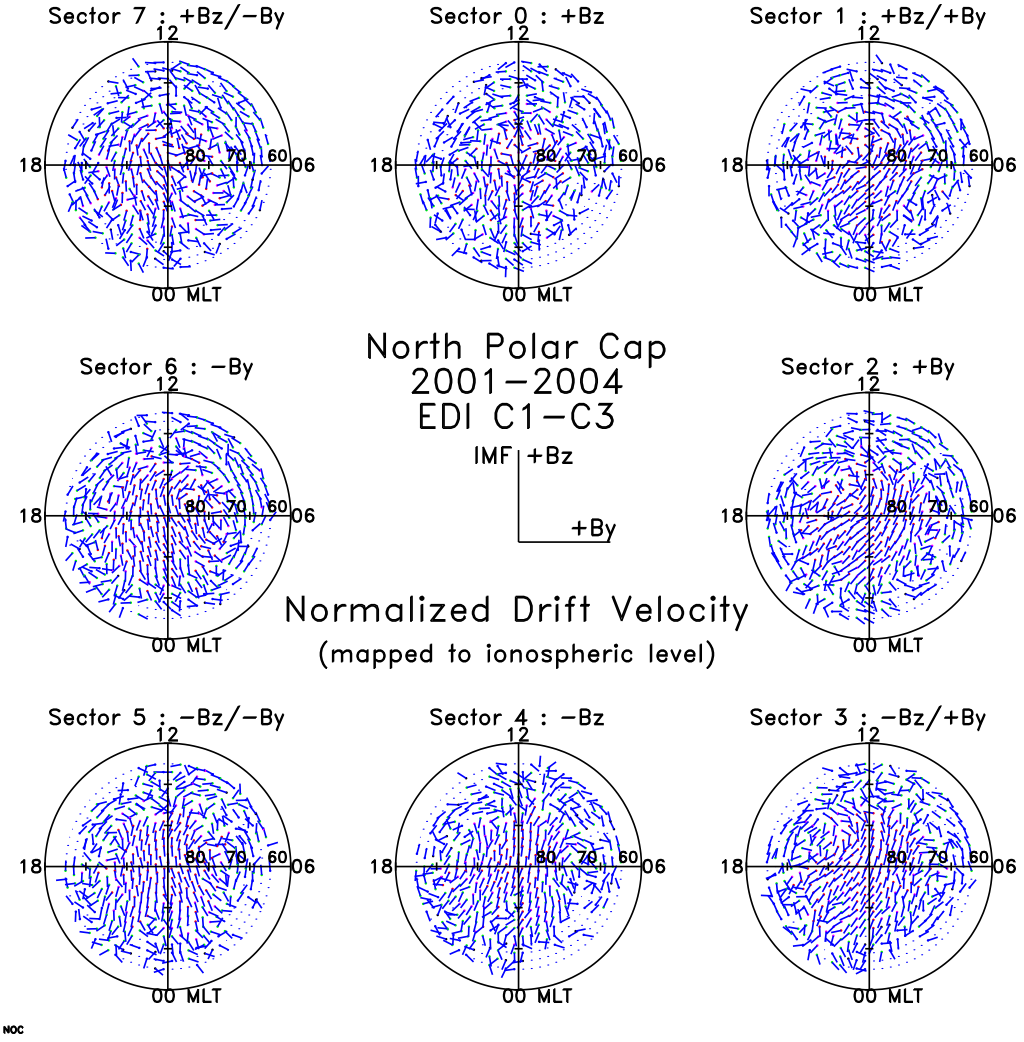

Figure 4. Drift patterns of mapped (into the Northern hemisphere) EDI drift measurements for all eight sectors of the IMF vector clock dial diagram. Normalized unit vectors of the drift are shown. The circles indicate $60°$-$90°$ *magnetic latitude versus MLT while the data binning reach till* $64°$.

Cluster became operational since 1 February 2001. In this preliminary statistical study we summarize the first four years between 2001–2004 of continuous observations with three of the four EDI probes in orbit; EDI onboard Cluster–4 was inoperational since early 2001. All together we used 2876 polar cap overflights (1459 north and 1417 south passages) for the statistical analysis of the drift behaviour in that spacious area. We used 1-min-averages of EDI observations (SP data). The averages were only calculated when at least four valid drift values with the highest quality stamp "good" were obtained within that minute and potentially erroneous data points with the poorest data quality level were discarded at all. This way the high-frequency noise was already filtered out which correspond to scale lengths smaller than about 250–300 km in space. The total number of data points amounts to nearly 3×10^5 for each hemisphere which corresponds to about 10^4 hours of observations all in all.

The data processing was done according to the following working steps. This description comprises also some aspects of the working plan which are to be implemented yet.

Step 1 : *Selection of EDI records.* Presently, 1-min averages from SP data are used. We eventually plan to use 10-min running averages of high resolution EDI primary parameter (PP) data classified as GOOD.

Step 2 : *Determining upstream solar wind condition.* The upstream solar wind conditions are important both for the convection and the mapping of drift vectors from Cluster EDI into the polar cap ionosphere. For this purpose, IMF data from the ACE spacecraft are time shifted so that they represent the IMF conditions just upstream of the subsolar magnetopause. The shifted IMF data are then used as input for the magnetic field mapping model. Later, the SW time delay will be calculated according to a scheme proposed by [4]. IMF data will then also be used for filtering the EDI data (next step).

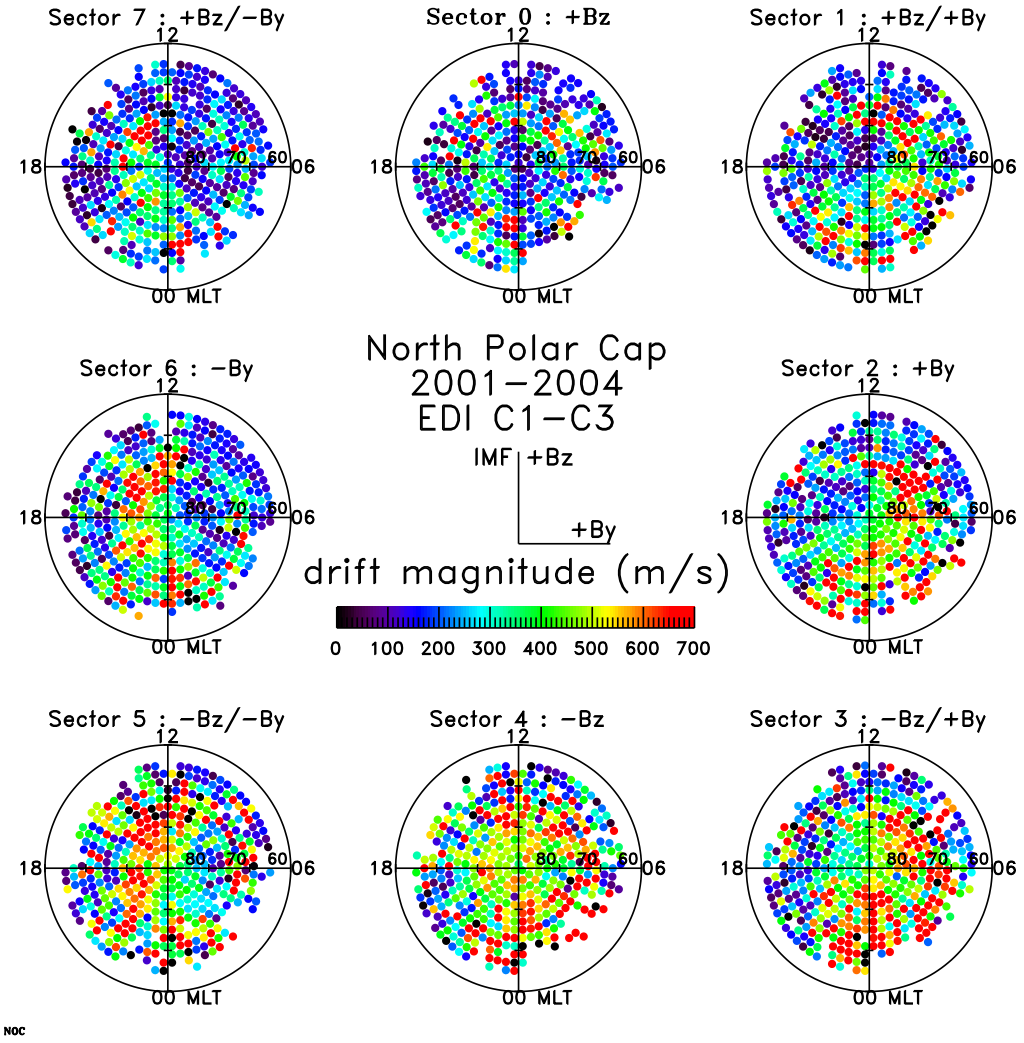

Figure 5. Statistical overview of the Northern hemisphere drift magnitude of mapped EDI drift measurements for all eight sectors (as in Fig. 4).

Step 3 : *Filtering according to IMF and and solar wind dynamic pressure* P_{dyn}. To remove intervals with too variable IMF, we compute the so-called bias vector, $\mathbf{B}_{bias}$, by taking all IMF y-z projections within a time interval τ , normalized to 1, and computing their average. Its magnitude, $|\mathbf{B}_{bias}|$, which ranges between 0 and 1, is a direct measure of the stability of the clock angle within τ. A similar filtering for variations in dynamic pressure is also planned.

Step 4 : *Binning according to IMF clock angle.* Based on the average IMF clock angle, we next bin the results into 8 different IMF sectors. The average direction of the bias vector determines the IMF sector.

Step 5 : *Mapping into the ionosphere.* For each remaining EDI measurement, the Cluster position is mapped into one of 522 grid positions, each cell approximately 200x200 km wide, in the polar cap ionosphere (i.e., magnetic latitudes poleward of 64 degrees). The mapping is done with the Tsyganenko–2001 magnetic field model [5, 6] and the input parameters for this model are obtained from ACE measurements (accordingly time shifted). Northern (Southern) hemisphere traversals are mapped to the Northern (Southern) hemisphere. The corresponding scaled EDI vector is also mapped to obtain the ionospheric drift vector.

Step 6 : *Averaging and statistical analysis.* Finally, an average drift vector for each IMF sector and grid position is obtained by averaging all vectors within the given sector and position. The variance in magnitude and direction are also calculated.

4. OBSERVATIONS

Fig. 3 shows one example of the drift pattern obtained. This is sector 3 ($135° \pm 22.5°$, $+B_y^{IMF}$ and $-B_z^{IMF}$) of the Northern hemisphere. The amount of data points within each bin is color-coded (scale on the left bottom).

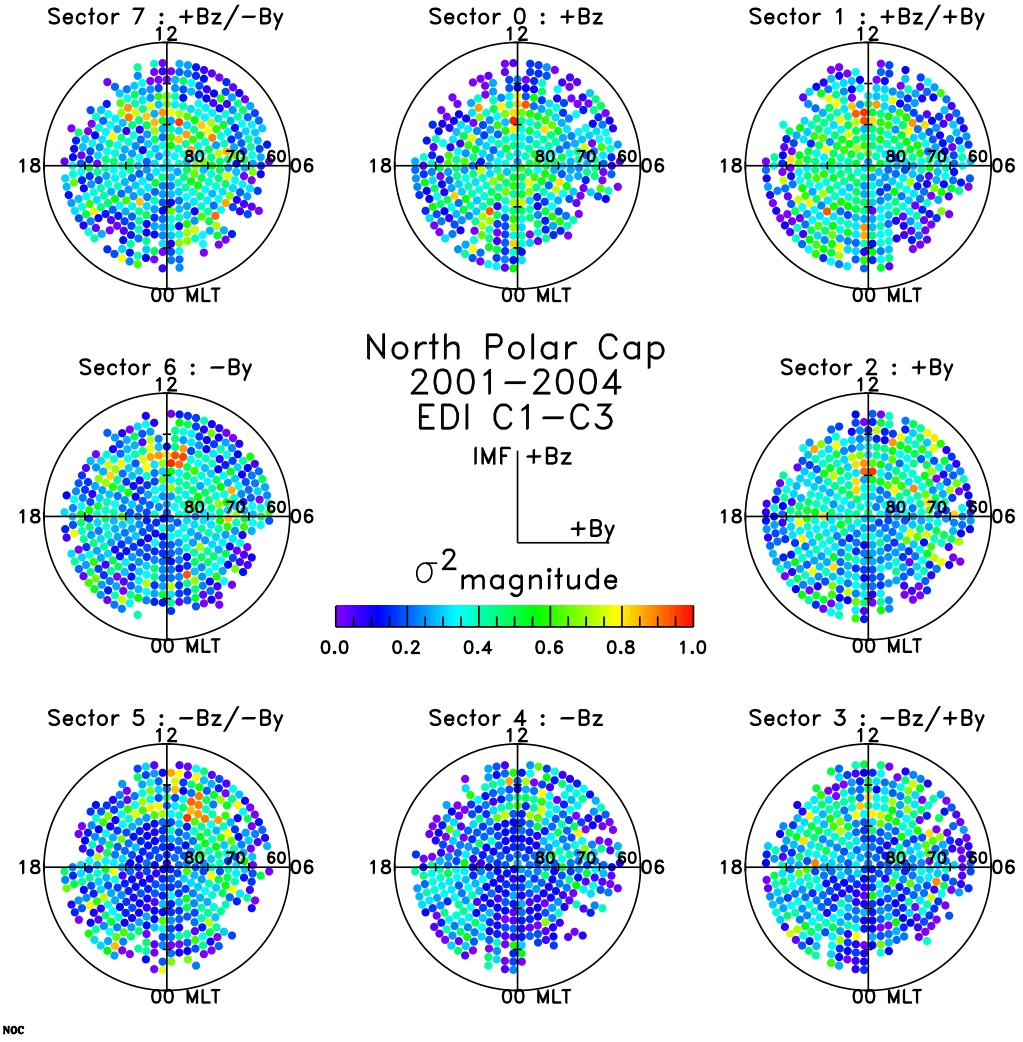

Figure 6. Statistical overview of the magnitude variance σ^2_{magn} of mapped EDI drift measurements for all eight sectors of the IMF vector clock dial diagram (as in Fig. 4). The variance is scaled from 0 to 1 (see color bar in middle panel).

It is high (> 100) in the central parts of the polar cap and decreases toward the edges. The arrows indicate the average maped drift vectors. The pattern shows a large convection cell in the dusk sector and a small and rather disturbed dawn cell with larger drift vectors (scale on the right bottom). The auroral ring is clearly visible as convection reversal zone and as a region of large drift vectors. Extraordinary large drift vectors are generally seen in the cusp region and on the nightside in the approximate position of the Harang discontinuity.

Overviews of Northern hemisphere drift patterns for all eight IMF sectors are shown in Figs. 4 and 5 with normalized drift vectors and colour-coded magnitude plots, respectively. The behaviour of the drift pattern in the central part of the polar cap, its variation with the IMF clock angle is quite similar to the well-known convection drift pattern of the models based on ground-based observations [as, e.g., 7, 8]. The detailed presentation of this is beyond the scope of this paper and will be shown elsewhere. In short, we observe a similar B_y^{IMF}-dependence of two-cell convection pattern and smaller, partly stagnant convection for northward IMF. The dusk convection cell is larger than the dawn cell for $+B_y^{IMF}$ as shown in the example of Fig. 3 and vice versa for predominance of $-B_y^{IMF}$. At the southern polar cap the patterns are reversed with respect to B_y^{IMF}-dependence. Because of the close similarity of the in-situ drift pattern with models from ground-based or low-Earth orbiting (LEO) satellites observations, we conclude that the central parts of the polar cap show predominantly quasi-steady conditions and allow to assume equipotentiality along the field lines, at least with respect to the large-scale convection structures.

Further, we used two different normalized variance parameters of the drift statistics. They are defined as follows.

$$\sigma^2_{total} = \frac{\langle|\mathbf{v}|^2\rangle - |\langle\mathbf{v}\rangle|^2}{\langle|\mathbf{v}|^2\rangle} \quad (1)$$

$$\sigma^2_{magn} = \frac{\langle|\mathbf{v}|^2\rangle - \langle|\mathbf{v}|\rangle^2}{\langle|\mathbf{v}|^2\rangle} \quad (2)$$

Metaphorically speaking, the first variance reflects the variability of the full vector variation, its degree of steady pointing direction (zero variance) or havily varying directions ($\sigma^2_{total} \rightarrow 1$). The second variance σ^2_{magn} gives the average deviation of the drift magnitude from its local average value.

The latter is shown here as an example in Fig. 6. The eight panels reveal a systematic pattern of the drift variance over the whole polar cap space in dependence of the IMF clock angle. This dependence is more striking for σ^2_{total}, where this variability approaches saturation values ($\rightarrow 1$) over large areas in a systematic way (not shown here). A small area at the position of the cusp region with large σ^2_{magn} values and obvious B_y^{IMF} and B_z^{IMF} dependences can be realized. The auroral ovals are clearly reproduced in all panels with varying width according to the different average disturbance level for the magnitude of the negative B_z^{IMF} component (larger toward the lower panels with sector numbers 3–5). Inside the polar cap, there appear additional regions of high variance which also depend on B_z^{IMF}, but also on the sign of the B_y^{IMF} component. The largest relative (normalized) variances within nearly the whole polar cap area (besides of the well-reflected cusp positions) are observed for sector 0 (purely $+B_z^{IMF}$, while for positive (negative) B_y^{IMF} the inner-polar-cap variance is shifted toward the afternoon/evening (morning/prenoon) sectors, extending up to the geomagnetic pole for the three upper panels (sectors 0, 1, and 7) and less far for the cases of increasing $-B_z^{IMF}$ component of the middle and lower panels. The largest area of continuous unidirectional flow over the polar cap is observed for sector 4 (pure negative B_z^{IMF}). At the southern hemisphere (not shown here) we observe a quite similar behaviour, but mirrored at the noon-midnight meridian in the same way as for the convection drift pattern.

The variance pattern within the polar cap space reflect obviously the predominant regions of active processes within the magnetosphere (auroral accelerations) and at the magnetopause (reconnection and/or flux transfer events with highly variable fast convection flows). For $+B_z^{IMF}$ conditions and in dependence of the B_y^{IMF} direction, they comprise more or less large areas of the polar cap space, the center of which are shifted toward the dawn or dusk side corresponding to the sign of B_y^{IMF} and oppositely directed at the opposite hemispheres.

5. SUMMARY

We performed a first preliminary statistical study of EDI electric drift measurements above the polar cap regions for the first four years (2001–2004) of Cluster's operation. Mapping the spatially distributed measurements to a common reference plane, in this case the ionospheric level, the resulting drift pattern inside the polar cap appears to vary with the IMF clock angle in a similar fashion as the well-known ground-based model representations. The two variance parameters σ^2_{total} and σ^2_{magn} show also a systematic variation with the IMF conditions revealing large areas of turbulent plasma convection at the dayside magnetosphere and shifted toward dawn or dusk for $-B_y^{IMF}$ or $+B_y^{IMF}$, respectively, at the northern hemisphere. This is mirror symmetric with respect to the noon-midnight meridian at the southern hemisphere. This variance and its IMF dependence should be communicated to the ionospheric level and it contributes there essentially to the high-latitude heating rates of the thermosphere and to particular large energy input (and corresponding temperature and density enhancement) within the projections of the cusp region. Further analysis of the large statistical basis is in progress and will be extended to correlations with further solar wind and geomagnetic parameters.

REFERENCES

[1] Kennel, C. F. *Convection and Substorms: Paradigms of Magnetospheric Phenomenology*, volume 2 of *International series on astronomy and astrophysics*. Oxford University Press, Inc., New York and Oxford, 1995.

[2] Vaith, H., Paschmann, G., Quinn, J. M., Förster, M., Georgescu, E., Haaland, S., Klecker, B., Kletzing, C. A., Puhl-Quinn, P. A., Réme, H., and Torbert, R. B. Plasma convection across the polar cap, plasma mantle and cusp: Cluster EDI observations. *Ann. Geophys.*, 22:2451–2461, 2004.

[3] Noda, H., Baumjohann, W., Nakamura, R., Torkar, K., Paschmann, G., Vaith, H., Puhl-Quinn, P., Förster, M., Torbert, R. B., and Quinn, J. M. Tail lobe convection observed by Cluster/EDI. *J. Geophys. Res.*, 108(A7):SMP 12(1–7), 2003.

[4] Weimer, D. R., Ober, D. M., Maynard, N. C., Collier, M. R., McComas, D. J., Ness, N. F., Smith, C. W., and Watermann, J. Predicting interplanetary magnetic field (IMF) propagation delay times using the minimum variance technique. *J. Geophys. Res.*, 108(A1):SMP–16(1–12), 2003.

[5] Tsyganenko, N. A. A model of the near magnetosphere with a dawn-dusk asymmetry 1. Mathematical structure. *J. Geophys. Res.*, 107(A8):SMP–12(1–17), 2002.

[6] Tsyganenko, N. A. A model of the near magnetosphere with a dawn-dusk asymmetry 2. Parameterization and fitting to observations. *J. Geophys. Res.*, 107(A8):SMP–10(1–17), 2002.

[7] Weimer, D. R. Models of high latitude electric potentials derived with a least error fit of spherical harmonic coefficients. *J. Geophys. Res.*, 100:19,595–19,602, 1995.

[8] Ruohoniemi, J. M. and Baker, K. B. Large-scale imaging of high-latitude convection with Super Dual Auroral Radar Network HF radar observations. *J. Geophys. Res.*, 103(A9):20,797–20,811, 1998.